第 42 卷第 5 期
2023 年 10 月

红 外 与 毫 米 波 学 报
J. Infrared Millim. Waves

Vol. 42, No. 5
October, 2023

文章编号：1001-9014(2023)05-0659-07

DOI:10. 11972/j. issn. 1001-9014. 2023. 05. 011

High performance and broadband photodetectors based on SnS_2/InSe heterojunction

WANG Bing-Hui[1,2], XING Yan-Hui[1*], HE Wen-Xin[1,2], GUAN Bao-Lu[1], HAN Jun[1], DONG Sheng-Yuan[1,2], LI Jia-Hao[1,2], FANG Pei-Jing[2], HAN Zi-Shuo[1], ZHANG Bao-Shun[2], ZENG Zhong-Ming[2*]

(1. Key Laboratory of Opto-electronics Technology, Ministry of Education, College of Microelectronics, Beijing University of Technology, Beijing 100124, China;
2. Nanofabrication facility, Suzhou Institute of Nano-Tech and Nano-Bionics, Chinese Academy of Sciences, Suzhou 215123, China)

Abstract: We reported a broadband photodetector with a spectral range of 365-965 nm, based on a SnS_2/InSe vertical heterojunction. In this device, InSe serves as the optical absorption layer, effectively extending the spectral range, while SnS_2 functions as the transmission layer, forming a heterojunction with InSe to facilitate separation of electron-hole pairs and enhance the responsivity. The photodetector exhibits a responsivity of 813 A/W under 365 nm. Moreover, it still maintained a high responsivity of 371 A/W, an external quantum efficiency of $1.3 \times 10^5\%$, a specific detectivity of 3.17×10^{12} Jones, and a response time of 27 ms under 965 nm illumination. The above investigation provides a new approach for broadband photodetectors with high responsivity.

Key words: two-dimensional material, heterojunction, Broadband photodetectors

基于SnS_2/InSe异质结的高性能宽带光电探测器

王冰辉[1,2]，邢艳辉[1*]，贺雯馨[1,2]，关宝璐[1]，韩 军[1]，董晟园[1,2]，李嘉豪[1,2]，方佩景[2]，韩梓硕[1]，张宝顺[2]，曾中明[2*]

(1. 北京工业大学 微电子学院 光电子技术教育部重点实验室，北京 100124；
2. 中国科学院 苏州纳米技术与纳米仿生研究所 纳米加工平台，江苏 苏州 215123)

摘要：我们报道了一种基于SnS_2 / InSe垂直异质结的宽带光电探测器，其光谱范围为365-965 nm。其中，InSe作为光吸收层，有效扩展了光谱范围，SnS_2作为传输层，与InSe形成异质结，促进了电子-空穴对的分离，增强了光响应。该光电探测器在 365 nm 下具有813 A/W 的响应度。并且，在965nm光照下它仍然具有371 A/W的高响应度，$1.3\times10^5\%$的外量子效率，3.17×10^{12} Jones的比探测率，以及27 ms的响应时间。该研究为高响应宽带光电探测器提供了一种新的方法。

关 键 词：二维材料；异质结；宽带光电探测器

中图分类号：TN214　　**文献标识码**：A

Introduction

Photodetectors play an important role in many fields such as remote sensing, reconnaissance, thermal imaging, and medical imaging. Narrow-spectrum photodetectors are unable to meet the increasingly complex needs of photodetection. The two-dimensional (2D) materials have received a lot of attention because of their unique structural, electrical and optical properties since the successful exfoliation of graphene in 2004[1-4]. Up to now, most of the reported photodetectors based on 2D materials work in a narrow spectral band[5], and there are relatively few reports on broadband photodetectors, which affect the development of 2D material photodetectors. In recent

Foundation items: This work is supported by the National Natural Science Foundation of China (61574011, 60908012, 61575008, 61775007, 61731019, 61874145, 62074011, 62134008), the Beijing Natural Science Foundation (4182015, 4172011, 4202010) and Beijing Nova Program (Z201100006820096) and International Student related expenses-Department of Information (040000513303).

Biography: WANG Bing-Hui (1998-), male, Handan, China, Master of Engineering. Research area involves two-dimensional materials, photodetectors. E-mail: wiceh610@163. com

[*] **Corresponding author**: E-mail: xingyanhui@bjut. edu. cn; zmzeng2012@sinano. ac. cn

years, InSe has been widely reported for its wide adjustable band gap ranging from 1.25 eV for bulk materials to 2.2 eV for monolayer materials[6]. InSe-based photodetectors are very suitable for the detection in the spectral range of 400-1 000 nm[7, 8], and InSe has high carrier mobility and small effective mass of electrons[9], all of which indicate that InSe is a promising candidate material for broadband response. However, the reported broadband InSe-based photodetectors have shown relatively low responsivity. For example, the WS_2/InSe heterojunction photodetector has a responsivity of 61 mA/W under 520 nm illumination[10]. The SnSe/InSe heterojunction photodetector has a responsivity of 350 mA/W under 808 nm illumination[11]. SnS_2 is an environment-friendly material with high carrier mobility, high switching ratio, and strong optical absorption, which makes it very suitable for photoelectric devices[12, 13]. However, the drawbacks of narrow spectrum response range of SnS_2 and the easy recombination of photogenerated carriers[14] have hindered its development. By combining the advantages of these two materials, it's promising to construct a broadband.

In this work, a SnS_2/InSe vertical structure photodetector was prepared, in which InSe was used as the photo absorption layer and SnS_2 was used as the transmission layer. By building a Van der Waals (vdW) heterojunction to form an effective type-II energy band alignment structure, the electron-hole pairs can be separated effectively to extend the carrier lifetime and improve the responsivity. The device had excellent responsivity in the 365-965 nm range, whose responsivity reached 813 A/W under 365 nm illumination with gate voltage modulation. Under the same gate voltage, a maximum responsivity of 371 A/W under 965 nm illumination, which was much higher than other reported broadband photodetectors[15], was obtained. And the device had a specific detectivity of 3.17×10^{12} Jones, a high external quantum efficiency of $1.3\times 10^{5}\%$ and a response time of 27 ms. These results demonstrate the successful preparation of a broadband SnS_2/InSe heterostructure photodetector with high performance.

2 Experimental section

2.1 Device fabrication

The SnS_2/InSe heterojunction device was fabricated on SiO_2/ Si substrates using a dry transfer technique. Firstly, few-layer flakes of SnS_2 and InSe were mechanically exfoliated from commercial bulk crystals, and the exfoliated SnS_2 flakes were transferred onto a highly p-doped Si substrate with 300 nm SiO_2, subsequently. The same approach was then adopted to transfer the exfoliated InSe onto SnS_2 with the assistance of an optical microscope (OM, BX51, OLMPUS). Finally, electrode patterns were prepared by electron-beam lithography system (EBL, Raith eLINE Plus) and then Ti/Au (10 nm/50 nm) metal stacks were deposited by electron beam evaporation (Ulvac Ei-5z) to form source and drain electrodes. Then Raman spectrometer (LABRAM HR, Japan Horriba-JY) and atomic force microscopy (AFM, Dimension ICON, American Bruker) were used to measure characteristic peaks and heights of materials. The atomic structure features, the composition and element distribution of the heterojunction were analyzed by high-resolution transmission electron microscopy (HRTEM, Talos) and energy dispersive X-ray spectroscopy (EDS), respectively.

2.2 Result and Discussion

Figure 1(a) shows the schematic diagram of a SnS_2/InSe heterojunction photodetector. The mechanically exfoliated SnS_2 and InSe were sequentially covered on the SiO_2/Si substrate, and the Ti/Au electrodes were placed on the SnS_2. Figure 1(b) shows the Raman spectrum of the single SnS_2 and InSe as well as the region where the two were stacked to form a heterojunction. The single SnS_2 [16] (blue line) had a typical Raman feature main peak A_{1g} at 313.4 cm^{-1}, and the single InSe [6] (red line) had four Raman feature peaks at 116 cm^{-1}, 178 cm^{-1}, 200 cm^{-1}, and 227 cm^{-1}, corresponding in turn to A_1', E" (TO), E" (LO), and A_1. All the above peaks were observed in the overlapping region of the SnS_2/InSe heterojunction (black line), indicating the formation of a Van der Waals heterojunction. The thicknesses of the SnS_2 and InSe were measured by AFM, as shown in Figure 1 (c). The thicknesses of SnS_2 and InSe were 12 nm and 10 nm, respectively, and the inset shows the surface topography of the heterojunction. Figure 1(d) shows the surface scanning electron microscope (SEM) image of the device, which had a regular shape and a contamination-free surface. The HRTEM characterized the interface of each layer of the device, as shown in Figure 1 (e). The interface of each layer of the device was clearly discernible and flat. Figure 1(f) shows the energy dispersive x-ray spectroscopy (EDS) of the device. The elements In, Se and S were uniformly distributed and no diffusion. Weak Sn elements signals was detected in the InSe layer, because Se and In are in adjacent positions in the periodic table, and the Sn-Lα peak overlaps with the In-Lβ peak, so the In-Lβ peak is sometimes mistaken for the Sn-Lα peak when detecting Sn element, so that it can be detected in the InSe layer. In fact, the Sn element was only detected in the bottom layer. All the above results indicate the successful fabrication of the high-quality SnS_2/InSe heterojunction.

Photoelectric characteristics of the SnS_2/InSe heterojunction photodetector was tested. Figure 2(a) shows Schematic diagram of the device measure setup. Bias voltages were applied to the electrodes connected to the SnS_2. Gate voltage (V_g) were applied through the highly doped silicon substrate. Figure 2(b) shows the output characteristic curves of the photodetector as the gate voltage varied from -60 V to 60 V under dark conditions. The inset was the output characteristic curves of SnS_2. Source-drain current (I_{ds}) increased with increasing gate voltage, indicating that the photodetector had effective gate voltage modulation. We thought that the nonlinear output curves of the SnS_2/InSe photodetector is mainly due to the additional barrier of heterojunction[6]. Figure 2 (c) shows the transfer characteristic curves of the photodetector. As the gate voltage changed from -80 V to 80 V, the device switched from the insulating state to the

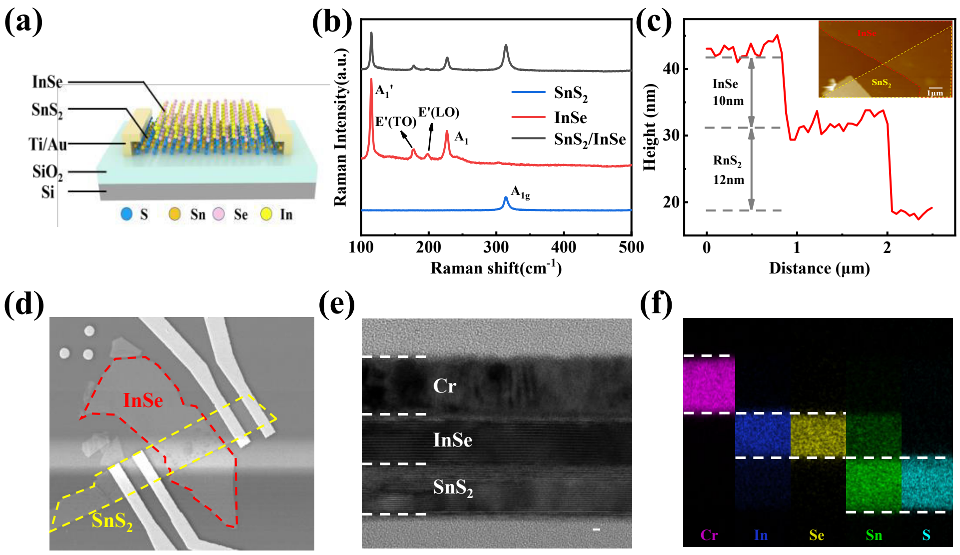

Fig. 1 (a) Schematic diagram of SnS_2/InSe heterostructure. (b) Raman spectrum of the single SnS_2, single InSe and their overlapped regions. (c) Height measurement maps of SnS_2 and InSe flakes in AFM, with insets showing the topographic views of SnS_2/InSe devices. (d) The SEM image of the SnS_2/InSe device. (e) HRTEM image, scale bar: 1 μm. (f) EDS image of each layer element.
图1 (a) SnS_2/InSe异质结构示意图,(b)单一SnS_2、单一InSe以及重叠区域的拉曼光谱图,(c)AFM测量的SnS_2和InSe薄片的高度图,插图为SnS_2/InSe器件的表面形貌,(d) SnS_2/InSe器件的SEM图像,(e) HRTEM图像,比例尺为1微米,(f)各层元素的EDS图像

conducting state. Figure 2(d) shows a plot of the logarithmic curves of I_{ds} versus V_g when source-drain voltage (V_{ds}) was 5 V, which characterized the switching ratio of the photodetector, and the switching ratio could reach 10^5, which indicated the device had good current regulation capability. Figure 2(e) shows the output characteristic curves at different incident optical power densities under 365 nm illumination when the gate voltage was 0 V. I_{ds} increased as the incident optical power density increased. Because with the increase of incident optical power density, more photogenerated carriers are generated in the channel, which lead to I_{ds} increase. To examine the gate voltage modulation capability of the device more intuitively, we tested the transfer characteristic curves at V_{ds}=5 V for different incident optical power densities. As shown in Figure 2(f), I_{ds} increased with increasing gate voltage, indicating that the gate voltage could effectively modulate the channel current, and a large gate voltage drive more photogenerated carriers through the heterojunction. In addition, I_{ds} increased with larger incident optical power density at the same gate voltage. Therefore, the large I_{ds} current was a result of the combined modulation of the gate voltage and the incident optical power density.

To characterize the detection performance of the SnS_2/InSe heterojunction photodetector under 365 nm illumination, the responsivity (R), specific detectivity (D*), external quantum efficiency (EQE), and noise equivalent power (NEP) were calculated according to the following equations:

$$R = I_{ph}/(P_{in}A) \quad , \quad (1)$$

$$D^* = RA^{1/2}/(2eI_{dark})^{1/2} \quad , \quad (2)$$

$$EQE = hcR\lambda^{-1}e^{-1} \quad , \quad (3)$$

$$NEP = A^{1/2}/D^* \quad , \quad (4)$$

where P_{in}, A, e, h, c, and λ are the incident optical power density, effective illuminated area, electron charge, Planck's constant, light speed, and incident light wavelength, respectively.

Figure 3(a) shows the photocurrent I_{ph}-V_g curves of the device. I_{ph} increased first and then decreased with increasing gate voltage. Figure 3(b) shows the responsivity dependence of the gate voltage under various incident power densities at V_{ds} = 5 V. The responsivity decreased with the increase of the incident optical power density. The highest responsivity of 813 A/W was obtained for the photodetector at P_{in}=1.269 mW/cm^2 and V_g=12.5 V. The high responsivity of the device is due to the large number of photogenerated carriers generated in InSe under illumination, which are attracted to the SnS_2 layer by the gate voltage, thereby increasing the current in SnS_2 and improving the responsivity of the photodetector. Figure 3(c) shows the specific detectivity and noise equivalent power of the photodetector at V_{ds}=5 V and V_g=0 V. The specific detectivity reached a maximum value of 6.74×10^{12} Jones at P_{in}=1.269 mW/cm^2 and the noise equivalent power reached a maximum value of 9.1×10^{-16} W/Hz$^{1/2}$ at P_{in}=16.75 mW/cm^2. Figure 3(d) shows the external quantum efficiency of the detector at V_g= 12.5 V and V_{ds}=5 V, reaching a maximum of 2.8×10^5% at P_{in}=1.269 mW/cm^2.

The response time is an important parameter for evaluating the performance of the photodetector. Figure 4(a) showed the optical switching characteristic curve of

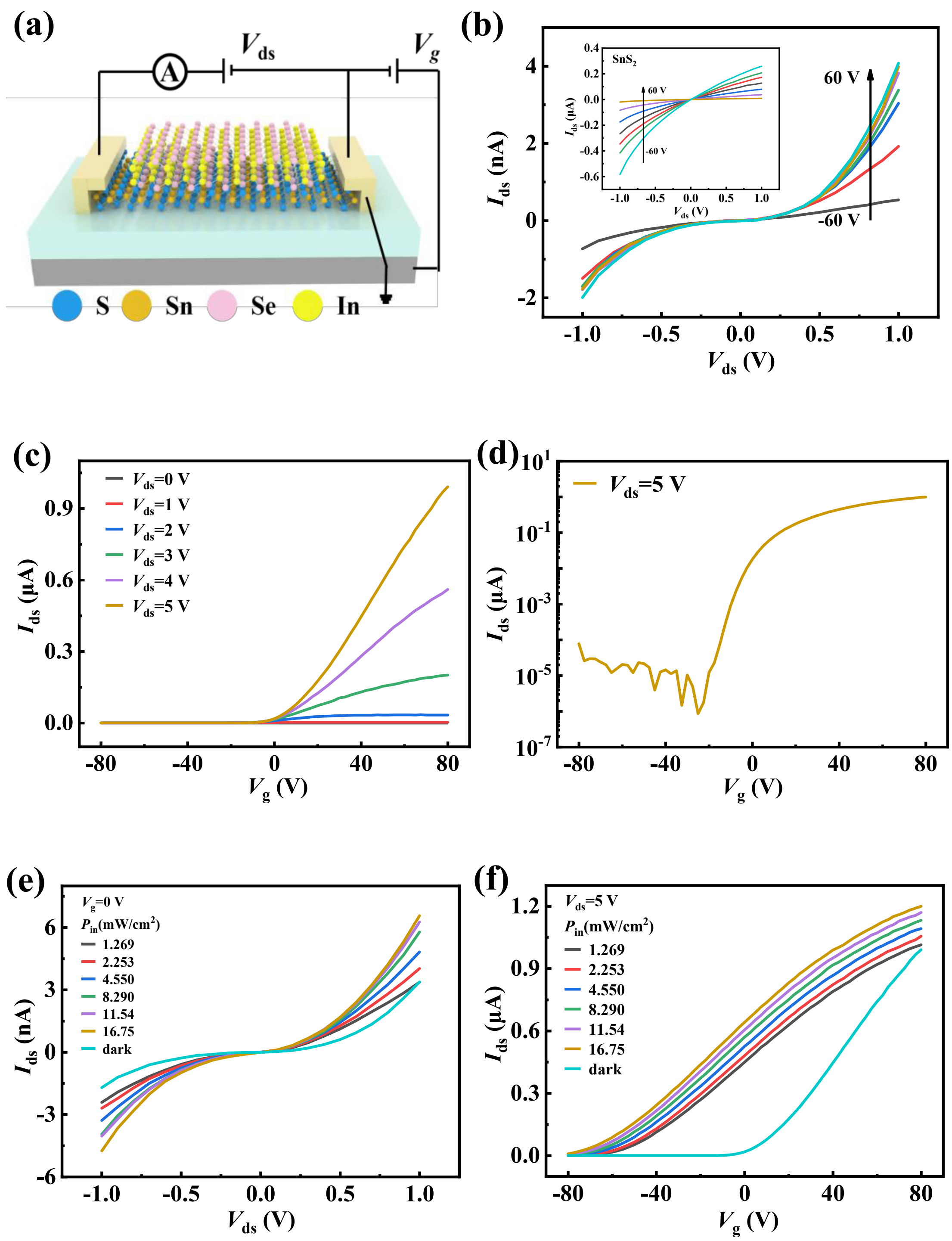

Fig. 2 (a) Schematic diagram of the device measure setup. (b) I_{ds}-V_{ds} output characteristic curves for different gate voltages under dark conditions (The inset was the output characteristic curves of SnS_2). (c) I_{ds}-V_g transfer characteristic curves for different source-drain voltage under dark conditions. (d) The logarithmic curves of I_{ds}-V_g when the source-drain voltage (V_{ds}) is 5 V. (e) Output characteristic curves for different incident optical power densities under 365 nm illumination (V_g=0 V). (f) Transfer characteristic curves for different incident optical power densities under 365 nm illumination (V_{ds}=5 V).

图2 (a)器件测试示意图,(b)黑暗条件下不同栅极电压的I_{ds}-V_{ds}输出特性曲线(插图是SnS_2的输出特性曲线),(c)黑暗条件下不同源漏电压的I_{ds}-V_g转移特性曲线,(d)源漏电压(V_{ds})为5V时I_{ds}-V_g的对数曲线,(e)在365nm光照下不同入射光功率密度的输出特性曲线(V_g=0 V),(f) 在365nm光照下不同入射光功率密度的转移特性曲线(V_{ds}=5 V)

the SnS_2/InSe heterojunction photodetector under 365 nm illumination. I_{ds} did not decay significantly after several times of optical switching, which indicated that the device had good stability. Figure 4(b) showed the response

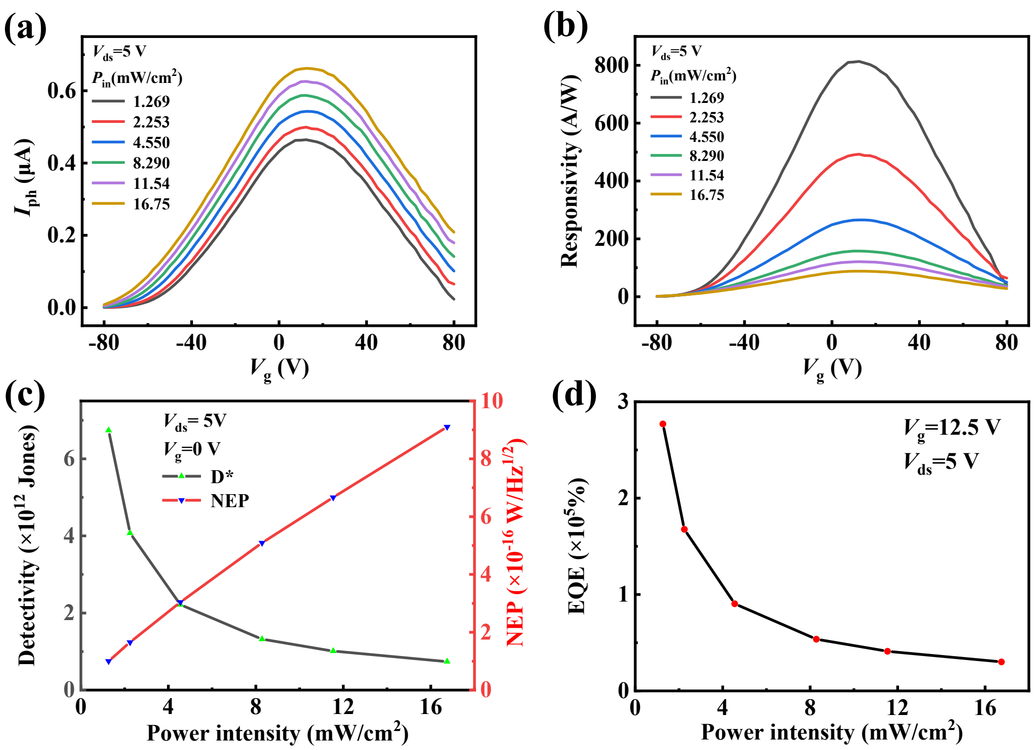

Fig. 3 SnS_2/InSe heterojunction photodetector under 365 nm illumination. (a) I_{ph} as a function of incident optical power density and gate voltage (V_{ds}=5 V). (b) Responsivity as a function of gate voltage for different incident optical power densities. (c) Detectivity and noise equivalent power as functions of incident optical power density. (d) External quantum efficiency as a function of incident optical power density.
图3 365nm光照下的SnS_2/InSe异质结光电探测器(a)不同入射光功率密度下的I_{ph}与栅极电压的函数关系(V_{ds}=5 V),(b)不同入射光功率密度的响应度与栅极电压的函数关系,(c)探测率和噪声等效功率与入射光功率密度的函数关系,(d)外量子效率与入射光功率密度的函数关系

time of the detector, where the rise time was about 27 ms and the fall time was about 54 ms.

In addition, the device had a high optical responsivity and sensitivity from UV to NIR. Figure 5(a) showed the optical switching characteristic curves of the device under the incident wavelength of 365-965 nm. I_{ds} of the device could change stably after several times of optical switching under different wavelength irradiation, which proved that the device had good detection for broadband, and the response time was also stable at about 27 ms. What's more I_{ds} was negatively correlated with wavelength, which is due to the fact that shorter wavelength light had higher energy. To verify the reliability of the experiment, we plotted the 2D image of the variation of responsivity with gate voltage at the same light power, as shown in Figure 5(b). The responsivity could also reach

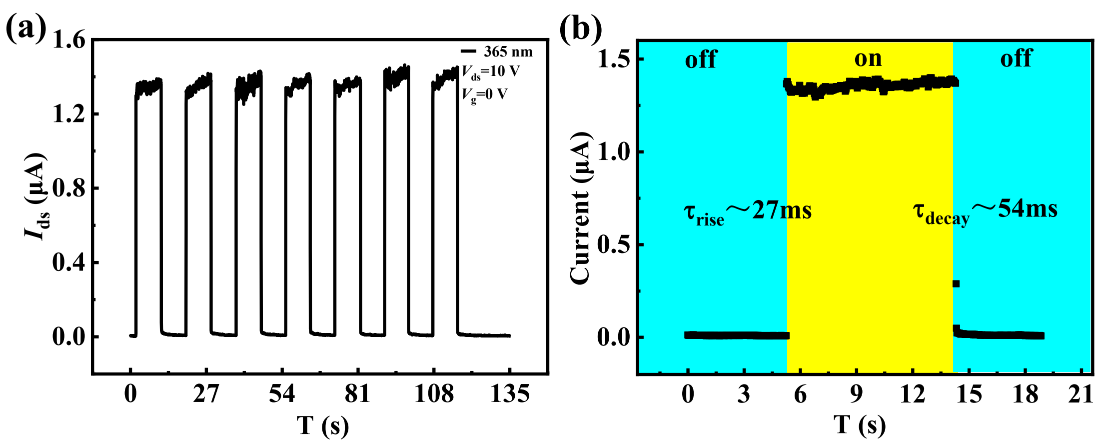

Fig. 4 (a) Optical switching characteristic curve under 365nm illumination. (b) Rise and fall time of photocurrent under 365nm illumination.
图4 (a)365nm光照下的光开关特性曲线,(b)365nm光照下光电流的上升和下降时间

371 A/W at V_g=12.5 V under 965 nm illumination, which was much higher than other 2D broadband photodetectors[17-19]. The specific detectivity and noise equivalent power versus different incident light wavelengths were shown in Figure 5(c). The detectivity of the device were of the order of 10^{12} Jones in the spectral range of 365-965 nm, and also 2-3 orders of magnitude higher than other 2D broadband photodetectors[10, 19, 20]. And the noise equivalent power were as low as 10^{-16} W/Hz$^{1/2}$. Figure 5(d) showed the external quantum efficiency versus the incident light wavelength, and a photovoltaic conversion capacity of 1.3×10^5% was also obtained under 965 nm illumination. Therefore, our device had a good optical response performance in the 365-965 nm broadband spectral range.

To compare with other broadband heterojunction photodetectors, table 1 lists the results of other research groups[11, 21-28]. According to the comparison and analysis in the table. SnS_2/InSe has excellent photoelectric performance, and it provides a direction for improving the comprehensive performance of the broadband photodetector.

3 Conclusion

In summary, we have successfully prepared a SnS_2/InSe photodetector. Using the wide band gap of InSe, the photodetector could detect the spectral range from UV to NIR. The device achieved a high responsivity of 813 A/W and 371 A/W under 365 nm and 965 nm illumination, respectively, which was higher than some other reported 2D broadband photodetectors. And the detectivity were the order of 10^{12} Jones in the spectral range of 365-965 nm. The photodetector also had an external quantum efficiency of 1.3×10^5% and a response time of 27 ms under 965 nm illumination. The SnS_2/InSe heterojunction photodetector provides a new way for developing broadband and high responsivity photodetectors.

Acknowledgment

This work is supported by the National Natural Science Foundation of China (No. 61574011, 60908012, 61575008, 61775007, 61731019, 61874145, 62074011, 62134008), the Beijing Natural Science Foundation (No. 4182015, 4172011, 4202010) and Beijing Nova Program (Z201100006820096) and International Student related expenses-Department of Information (040000513303). The authors would like to thank the Nano Fabrication Facility, Vacuum Interconnected Nanotech Workstation at Suzhou Institute of Nano-Tech and Nano-Bionics, Chinese Academy of Sciences, and Laboratory of Nanodevices and

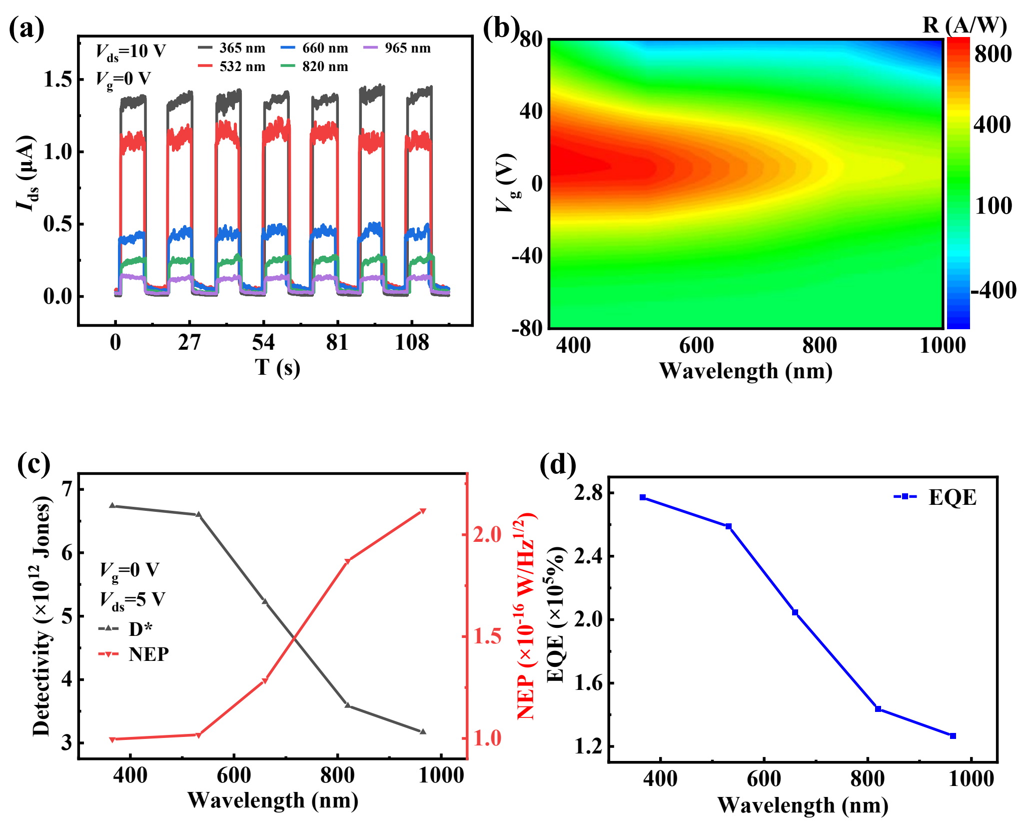

Fig. 5 (a) Optical switching characteristics under different incident light wavelength irradiation. (b) 2D images of responsivity as a function of gate voltage and incident light wavelength. (c) Detectivity and noise equivalent power as a function of incident light wavelength. (d) External quantum efficiency as a function of incident light wavelength.
图5 (a)不同入射光波长照射下的光开关特性,(b)响应度与栅极电压和入射光波长的2D函数图像,(c)探测率和噪声等效功率与入射光波长的函数关系,(d)外量子效率与入射光波长的函数关系

Table 1 Performance indicators comparison of this work with other typical photodetectors based on Se materials
表1　本工作与其他典型硒基光电探测器性能指标对比

Device	Laser λ (nm)	Responsivity (A/W)（MAX）	Rise/fall time (ms)	Detectivity（Jones）	Reference
MoS_2/BP/Si	532-1550	22.3/153.4×10^{-3}	15×10^{-3}	3.1×10^{11}/2.13×10^{9}	[21]
quasi-2D tellurium	520-3000	354/1.36×10^{3}	52.3×10^{-3}/64×10^{-3}	7.69×10^{11}	[22]
Bi_2Se_3	1456	2.7	500	3.3×10^{10}	[23]
2D-Te	1000-3500	27	~200	2.6×10^{11}	[24]
MoS_2/Si	532-808	0.975	6.8/6.7	6.56×10^{11}	[25]
BP/MoS_2	280-660	77.16	>50	6.5×10^{9}	[26]
Graphene/BP	655-980	55.75/0.66	36		[27]
bismuth selenide	532-1064	300	2×10^{3}	7.5×10^{9}	[28]
SnSe/InSe	405-808	0.35	260/170	5.8×10^{10}	[11]
SnS_2/InSe	365-965	813/371	27/54	6.74×10^{12}	This work

Applications, Suzhou Institute of Nano-Tech and Nano-Bionics, Chinese Academy of Sciences for their technical supports.

References

[1] Peng M Z, Cheng J D, Zheng X H, *et al*. 2D-materials-integrated optoelectromechanics: recent progress and future perspectives [J]. *Reports on Progress in Physics*, 2023, **86**(2).

[2] Wan W H, Guo R, Ge Y F, *et al*. Carrier and phonon transport in 2D InSe and its Janus structures [J]. *Journal of Physics-Condensed Matter*, 2023, **35**(13).

[3] Dai M J, Chen H Y, Wang F K, *et al*. Ultrafast and Sensitive Self-Powered Photodetector Featuring Self-Limited Depletion Region and Fully Depleted Channel with van der Waals Contacts [J]. *Acs Nano*, 2020, **14**(7): 9098-106.

[4] Wu G J, Wang X D, Chen Y, *et al*. $MoTe_2$ p-n Homojunctions Defined by Ferroelectric Polarization [J]. *Adv Mater*, 2020, **32**(16).

[5] Yadav S M, Pandey A. An efficient white-light photodetector based on 2D-SnS_2 nanosheets [J]. *IEEE Transactions on Electron Devices*, 2022, **69**(4): 1889-93.

[6] Ma H X, Xing Y H, Han J, *et al*. Ultrasensitive and Broad-Spectrum Photodetectors Based on InSe/ReS_2 Heterostructure [J]. *Advanced Optical Materials*, 2022, **10**(5).

[7] Cao R, Wang H D, Guo Z N, *et al*. Black Phosphorous/Indium Selenide Photoconductive Detector for Visible and Near-Infrared Light with High Sensitivity [J]. *Advanced Optical Materials*, 2019, **7**(12).

[8] Zhao S W, Wu J C, Jin K, *et al*. Highly Polarized and Fast Photoresponse of Black Phosphorus-InSe Vertical p-n Heterojunctions [J]. *Advanced Functional Materials*, 2018, **28**(34).

[9] Yang X, Liu Z, Gao F, *et al*. Mixed-dimensional InSe - Si heterojunction nanostructures for self-powered broadband photodetectors [J]. *ACS Applied Nano Materials*, 2021, **4**(12): 12932-6.

[10] Chen J P, Zhang Z, Ma Y, *et al*. High-performance self-powered ultraviolet to near-infrared photodetector based on WS_2/InSe van der Waals heterostructure [J]. *Nano Research*.

[11] Yan Y F, Abbas G, Li F, *et al*. Self-Driven High Performance Broadband Photodetector Based on SnSe/InSe van der Waals Heterojunction [J]. *Advanced Materials Interfaces*, 2022, **9**(12).

[12] Liu Z, Jia X Y, Duan W S, *et al*. High Photoresponsivity and Response Speed of Visible-Light Photodetectors Based on Tin Disulfide/Indium-Doped Tin Disulfide Homostructures [J]. *Advanced Optical Materials*, 2023, **11**(3).

[13] Zhao Y, Tsai T Y, Wu G, *et al*. Graphene/SnS_2 van der Waals Photodetector with High Photoresponsivity and High Photodetectivity for Broadband 365-2240 nm Detection [J]. *Acs Applied Materials & Interfaces*, 2021, **13**(39): 47198-207.

[14] Zhang H T, Li H W, Yu H, *et al*. High responsivity and broadband photodetector based on SnS_2/Ag_2S heterojunction [J]. *Materials Letters*, 2023, 330.

[15] Du C H, Gao H L, Du W T, *et al*. High responsivity and broadband polarized photodetectors based on InSe/$ReSe_2$ van der Waals heterostructures [J]. *Journal of Alloys and Compounds*, 2022, 919.

[16] Cui B Y, Han J, Xing Y H, *et al*. Ultrahigh Photoresponsive Photodetector Based on Graphene/SnS_2 van der Waals Heterostructure [J]. *Physica Status Solidi a-Applications and Materials Science*, 2021, **218**(21).

[17] Wan Z, Mu H, Dong Z, *et al*. Self-powered $MoSe_2$/ZnO heterojunction photodetectors with current rectification effect and broadband detection [J]. *Materials & Design*, 2021, **212**: 110185.

[18] Li X, Ruan S, Zhu H. SnS Nanoflakes/Graphene Hybrid: Towards Broadband Spectral Response and Fast Photoresponse [J]. *Nanomaterials*, 2022, **12**(16): 2777.

[19] Zhong J H, Wu B A, Madoune Y, *et al*. $PdSe_2$/$MoSe_2$ vertical heterojunction for self-powered photodetector with high performance [J]. *Nano Research*, 2022, **15**(3): 2489-96.

[20] Zhang X M, Yan C L, Hu X, *et al*. High performance mid-wave infrared photodetector based on graphene/black phosphorus heterojunction [J]. *Materials Research Express*, 2021, **8**(3).

[21] Ye L, Li H, Chen Z F, *et al*. Near-Infrared Photodetector Based on MoS_2/Black Phosphorus Heterojunction [J]. *Acs Photonics*, 2016, **3**(4): 692-9.

[22] Tong L, Huang X Y, Wang P, *et al*. Stable mid-infrared polarization imaging based on quasi-2D tellurium at room temperature [J]. *Nature Communications*, 2020, **11**(1).

[23] Wang F, Li L, Huang W, *et al*. Submillimeter 2D Bi_2Se_3 flakes toward high-performance infrared photodetection at optical communication wavelength [J]. *Advanced Functional Materials*, 2018, **28**(33): 1802707.

[24] Amani M, Tan C L, Zhang G, *et al*. Solution-Synthesized High-Mobility Tellurium Nanoflakes for Short-Wave Infrared Photodetectors [J]. *Acs Nano*, 2018, **12**(7): 7253-63.

[25] Guo L J, Gu Y S, Yang Z, *et al*. $CsPbBr_3$ QDs Modified Vertically Layered MoS_2/Si Heterojunction for Fast UV-vis-NIR Spectrum Flexible Photodetectors [J]. *Advanced Materials Interfaces*, 2021, **8**(7).

[26] Krishnamurthi V, Low M X, Kuriakose S, *et al*. Black Phosphorus Nanoflakes Vertically Stacked on MoS_2 Nanoflakes as Heterostructures for Photodetection [J]. *Acs Applied Nano Materials*, 2021, **4**(7): 6928-35.

[27] Xu J, Song Y J, Park J H, *et al*. Graphene/black phosphorus heterostructured photodetector [J]. *Solid-State Electronics*, 2018, **144**: 86-9.

[28] Sharma A, Bhattacharyya B, Srivastava A K, *et al*. High performance broadband photodetector using fabricated nanowires of bismuth selenide [J]. *Scientific Reports*, 2016, 6.